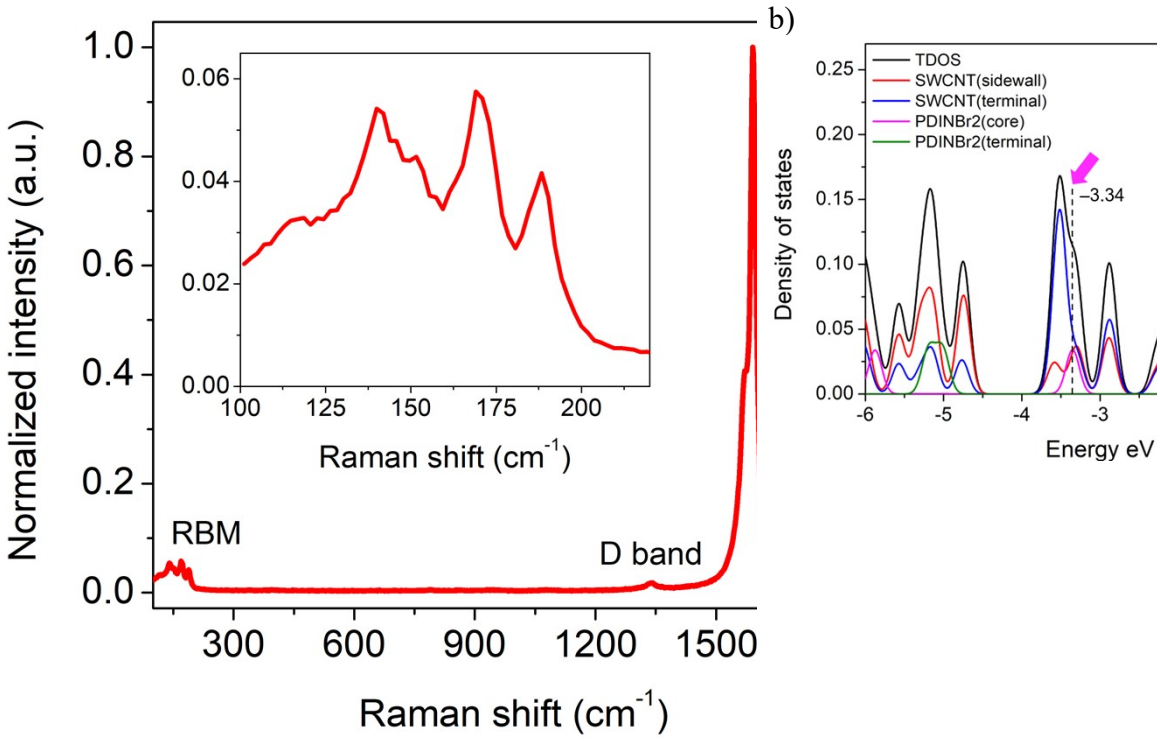

Figure A. The Raman spectrum of the SWCNT film, RBM modes (100 – 200 cm^{-1}) shown in the inset.

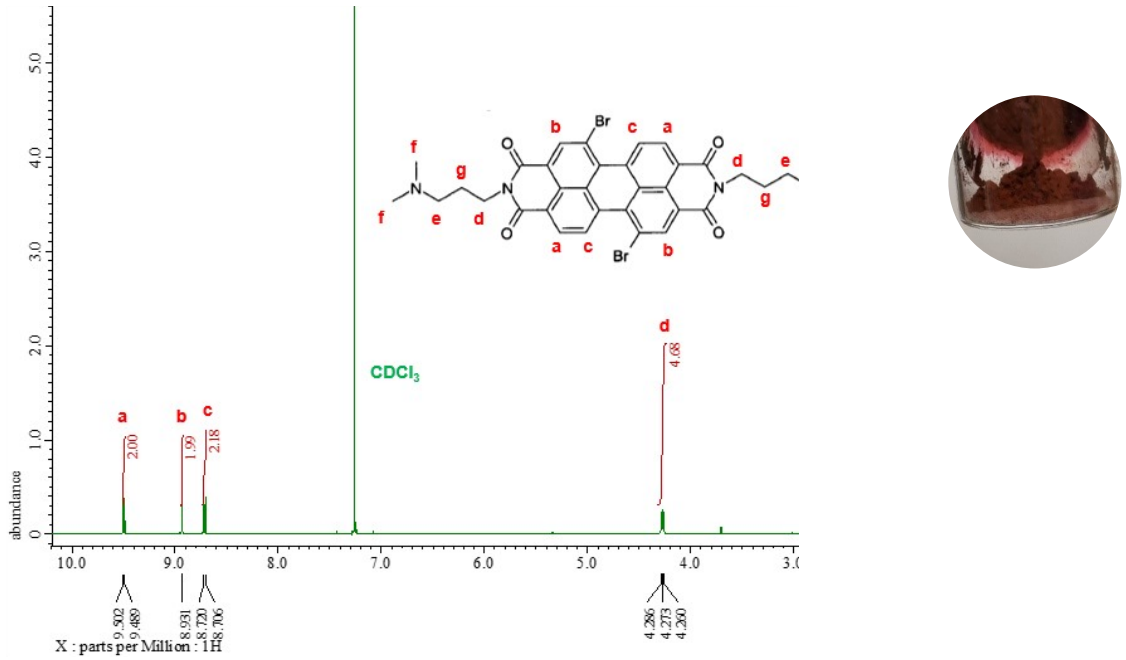

Figure B. The ^{1}H NMR spectra of $PDINBr_2$.

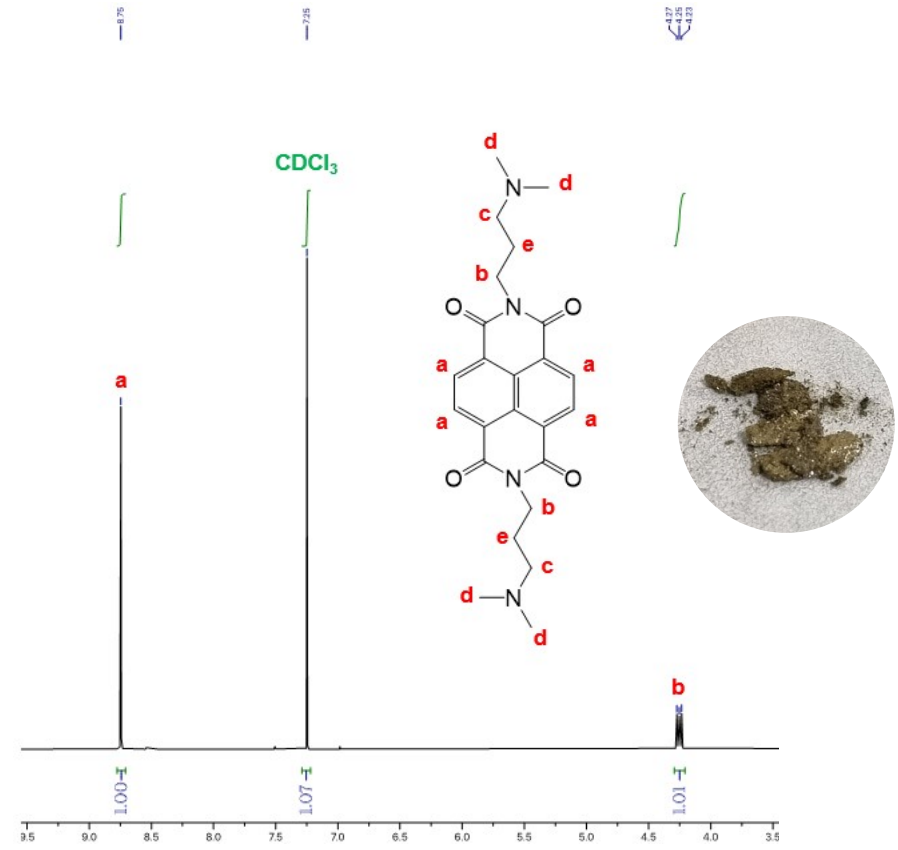

Figure C. The ^{1}H NMR spectra of NDIN.

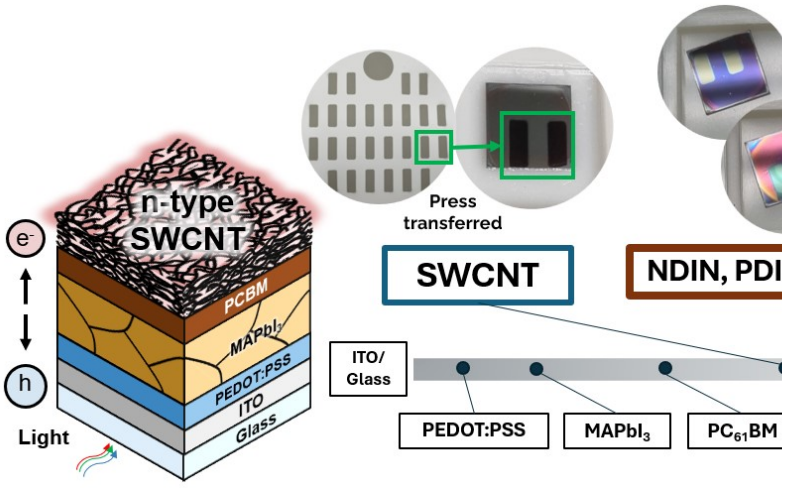

Figure D. Perovskite solar cell fabrication process.

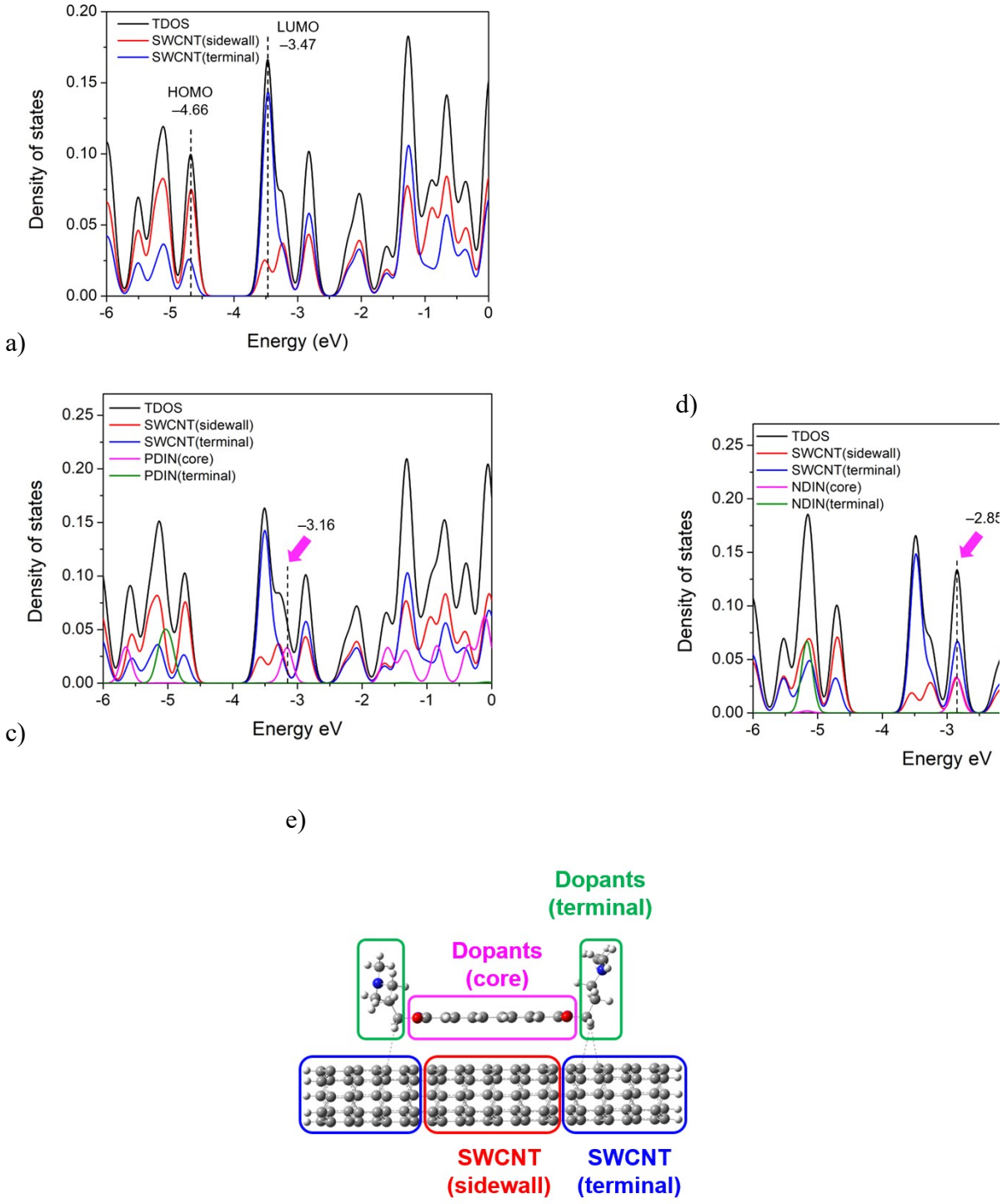

Figure S1. Partial density of states (PDOS) of (a) the pristine SWCNT, (b–d) SWCNT–dopant complexes, with the decomposition based on (c) the corresponding structural fragmentation.

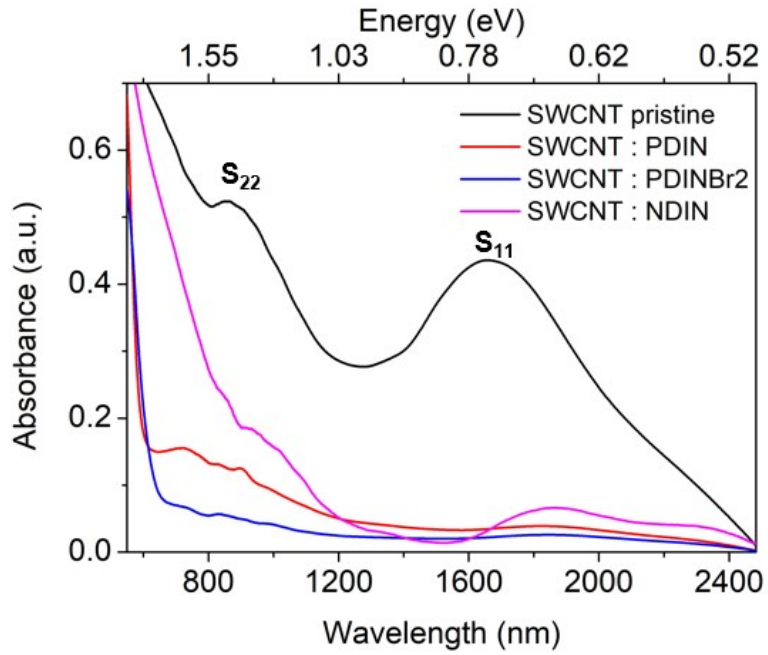

Figure S2. Near-infrared (NIR) absorption spectra of pristine and n-doped SWCNT films.

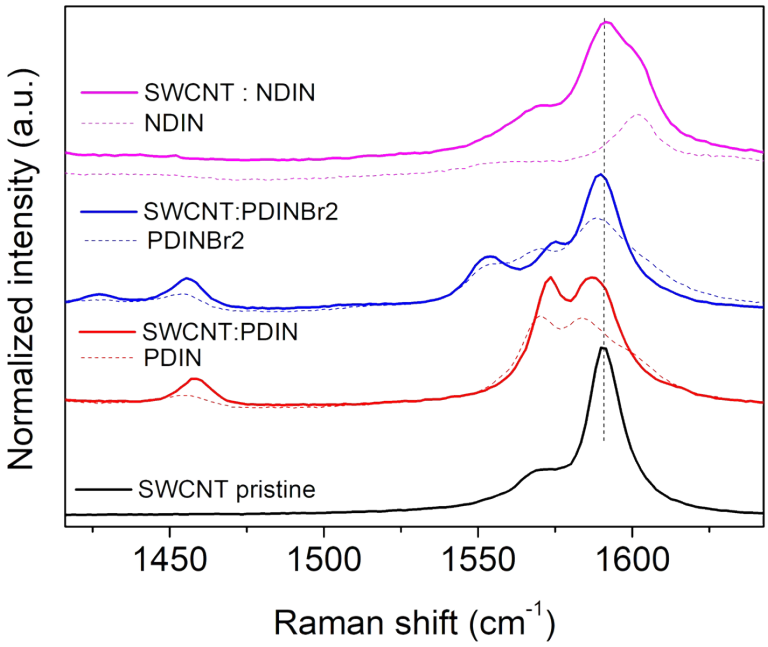

Figure S3. Raman spectra of pristine and n-doped SWCNT films compared to their corresponding dopants.

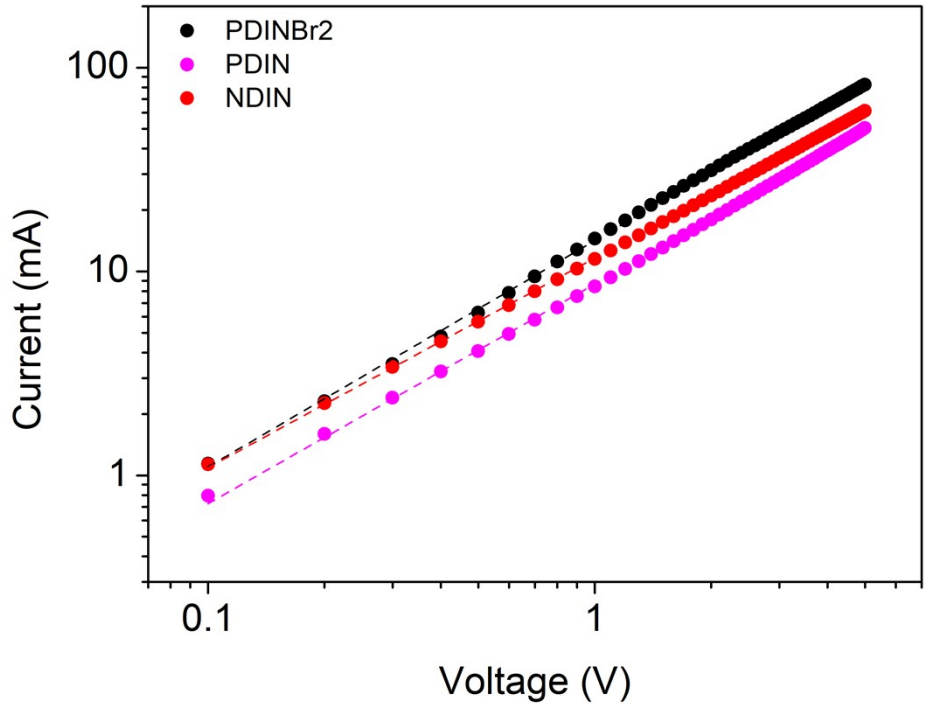

Figure S4. Dark log(*I*)–log(*V*) characteristics of ITO/SWCNT:dopant/Ag device. The trap-free SCLC region were fitted and their intercept was used to calculate the carrier mobility (μ).[9]

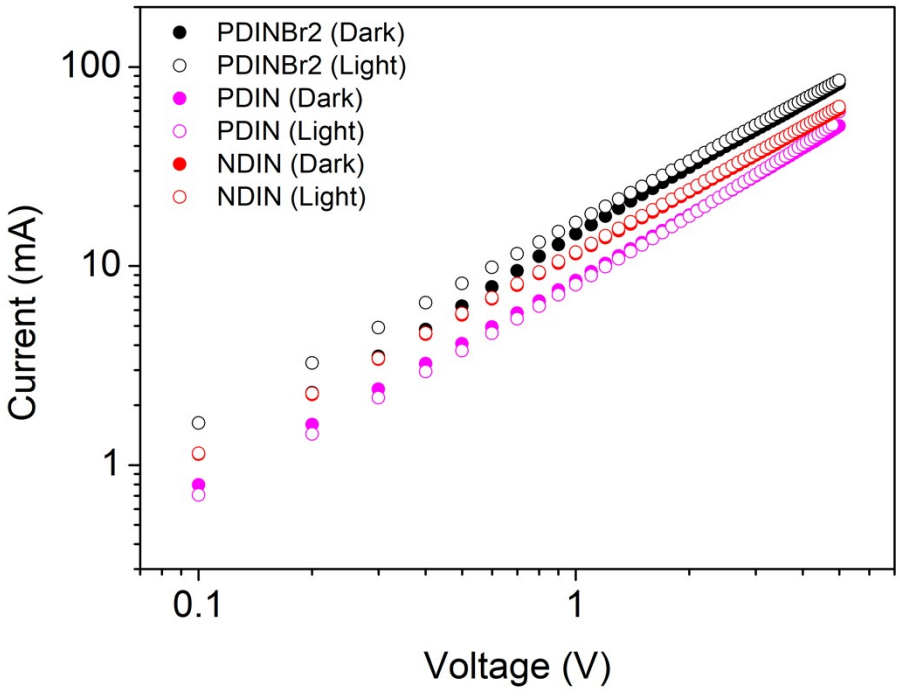

Figure S5. Dark current-voltage (*I–V*) plot of pristine and doped SWCNT films (with PDIN, $PDINBr_2$, and NDIN) measured under dark and illuminated (1 sun) conditions.

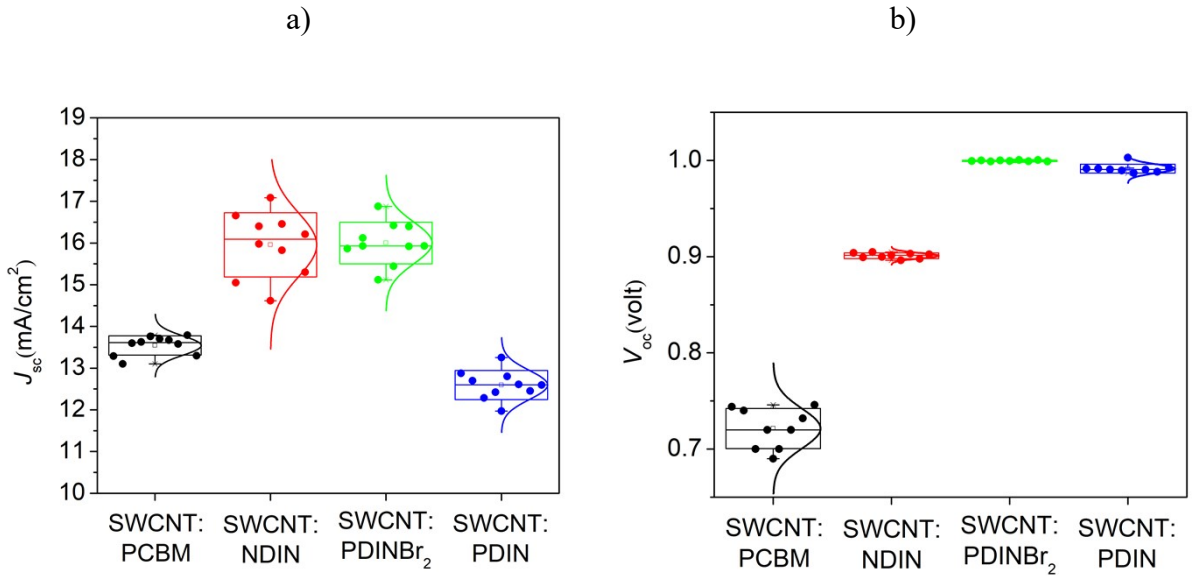

Figure S6. PSC device statistical distributions of (a) short-circuit current density, and (b) open-circuit voltage compared among dopants (n = 10).

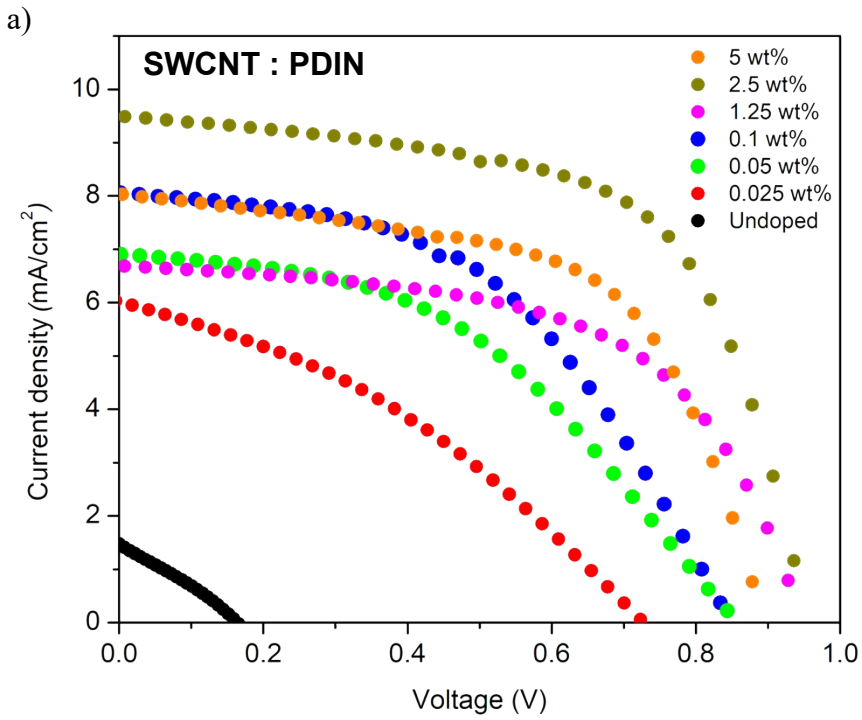

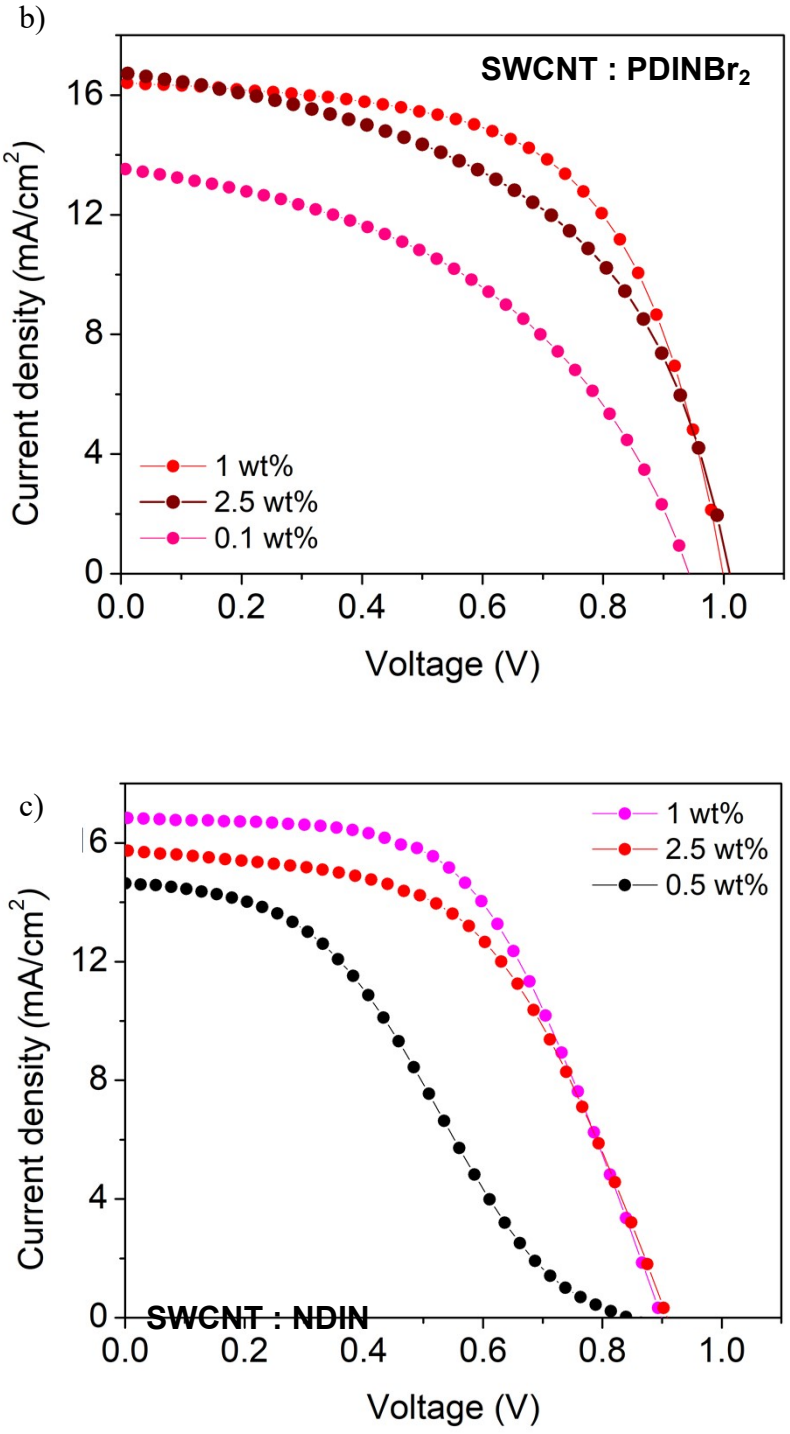

Figure S7. *J–V* characteristics of PSCs employing (a) PDIN, (b) $PDINBr_2$, and (c) NDIN-doped SWCNT cathodes with different dopant concentrations.

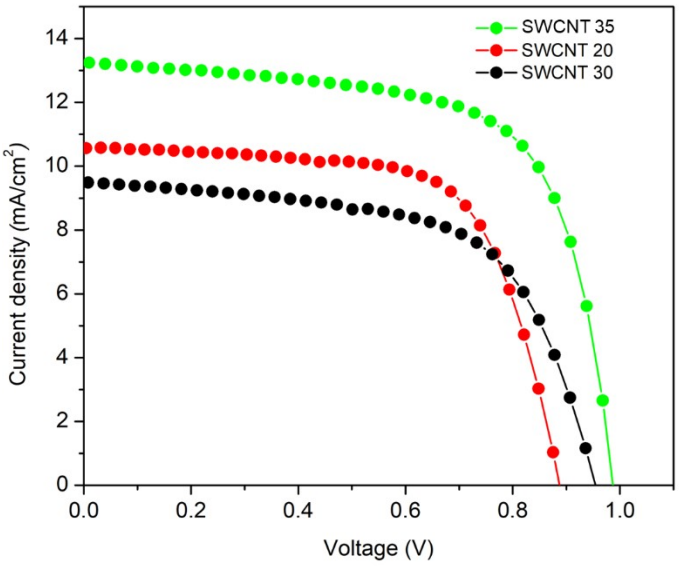

Figure S8. *J–V* characteristics of PSCs employing PDIN-doped SWCNT cathodes with different SWCNT transmittance (*T*) = 35%, 30%, and 20%.

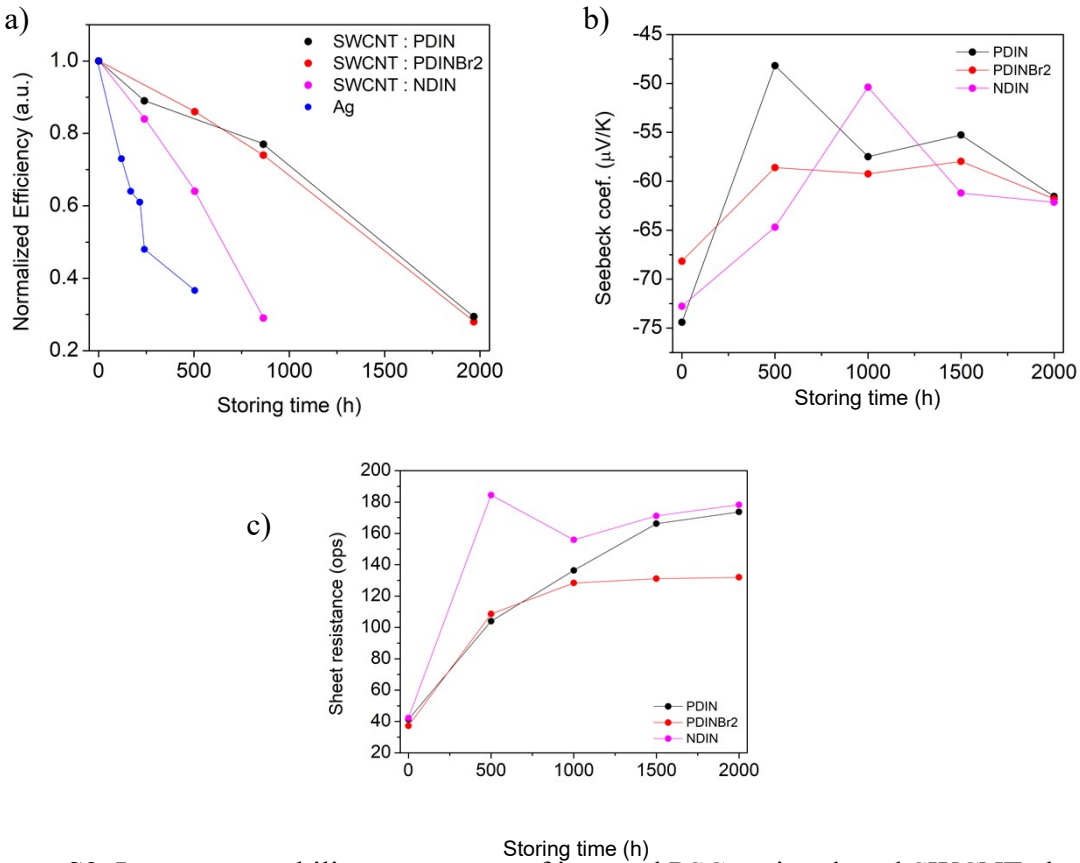

Figure S9. Long-term stability assessment of inverted PSCs using doped SWCNT electrodes (a) Normalized PCE, (b) *S*, and (c) R_{Sheet} of doped SWCNT films.